GEOPHYSICS, VOL. 53, NO. 9 (SEPTEMBER 1988); P. 1175–1183, 14 FIGS.

Three-dimensional acoustic modeling by the Fourier method

Moshe Reshef*, Dan Kosloff‡, Mickey Edwards§, and Chris Hsiung**

ABSTRACT

A three-dimensional forward modeling algorithm, allowing arbitrary density and arbitrary wave propagation velocity in lateral and vertical directions, directly solves the acoustic wave equation through spatial and temporal discretization. Spatial partial differentiation is performed in the Fourier domain. Time stepping is performed with a second-order differencing operator. Modeling includes an optional free surface above the spatial grid. An absorbing boundary is applied on the lateral and bottom edges of the spatial grid.

Three-dimensional forward modeling represents a challenge for computer technology. Computation of meaningfully sized models requires extensive calculations and large three-dimensional data sets which must be retrieved and restored during the computation of each time step. The computational feasibility of the Fourier method is demonstrated by implementation on the multiprocessor CRAY X-MP computer system using the large secondary memory of the solid-state storage device (SSD). Calculations use vectorization and parallel processing architecture. The similarity of numerical and analytical results indicates sufficient accuracy for many applications.

INTRODUCTION

Three-dimensional forward modeling is useful in the quality control and interpretation of three-dimensional (3-D) seismic surveys and may prove to be important in the understanding of wave propagation. For 3-D surveys over complicated geology, it is not simple to trace the origin of all recorded time section arrivals. To date, most truly heterogeneous 3-D seismic modeling has been performed with approximate methods based on geometrical optics (Hilterman, 1970). These methods are useful for a general evaluation but do not give accurate amplitudes and often break down completely near caustics. Three-dimensional ray tracing can also become unwieldy for realistic structures. On the other hand, potentially accurate direct methods such as finite-difference (Kelly et al., 1976), finite-element (Marfurt, 1984), or the Fourier method (Gazdag, 1981; Kosloff and Baysal, 1982) have been considered too expensive for 3-D seismic modeling. This paper demonstrates that, with the recent advances in supercomputer technology, such modeling is feasible today and could become commonplace in the near future.

From a mathematical viewpoint, the new algorithm resembles the two-dimensional (2-D) algorithm described in Kosloff and Baysal (1982). In particular, the solution scheme uses a spatial grid to discretize the geologic structure. Fast Fourier transforms (FFTs) are used for calculating spatial partial derivatives and time stepping is achieved by time integration of second-order differencing. Furthermore, all numerical stability and dispersion criteria obtained in the 2-D study are found to be suitable for the 3-D case. However, it must be mentioned that in the Fourier method neither free-surface boundaries nor material discontinuities are explicitly defined. A careful comparison with analytic solutions is always required. The Fourier method appears very suitable for 3-D modeling because it has the advantage of requiring a relatively small number of grid points to achieve a specified accuracy.

The main difficulty in designing the new forward modeling algorithm was the management of the extremely large volume of data required for the calculations. Typical forward modeling problems require tens of millions of words of storage, an amount which exceeds the central memory of most computer systems. The necessity of retrieving and restoring 3-D data sets for the computation of each of several thousand time steps leads to an input-output bound intractable or infeasible problem when conventional disk storage is contemplated. With the advent of the 128 million word and larger solid-state storage devices (SSDs), we have sufficient memory and input-output bandwidth to perform Fourier method forward modeling with meaningfully sized models. The capability of transferring more than two billion bytes per second to and from

Manuscript received by the Editor December 1, 1986; revised manuscript received February 29, 1988.
*Formerly Cray Research Inc., Houston; presently Department of Geophysics and Planetary Sciences, Tel Aviv University, Tel Aviv 69978, Israel.
‡Formerly Federal University of Bahia, Salvador, Bahia, Brazil; presently Department of Geophysics and Planetary Sciences, Tel Aviv University, Tel Aviv 69978, Israel.
§Cray Research Inc., 5847 San Felipe, Ste. 3000, Houston, TX 77057.
**Cray Research Inc., 900 Lowater Road, Chippewa Falls, WI 54729.

central memory negates the input-output obstacle and allows the design of a CPU bound algorithm.

THE ACOUSTIC WAVE EQUATION IN THREE DIMENSIONS

Wave propagation in a 3-D acoustic medium is described by the following:

$$\frac{1}{\rho C^2}\frac{\partial^2 P}{\partial t^2} = \frac{\partial}{\partial x}\left(\frac{1}{\rho}\frac{\partial P}{\partial x}\right) + \frac{\partial}{\partial y}\left(\frac{1}{\rho}\frac{\partial P}{\partial y}\right) + \frac{\partial}{\partial z}\left(\frac{1}{\rho}\frac{\partial P}{\partial z}\right) + S, \quad (1)$$

where t denotes time, $P(x, y, z, t)$ denotes the pressure, $C(x, y, z)$ is the velocity field, $\rho(x, y, z)$ is the density, and $S(x, y, z, t)$ denotes the source term which is derived from the divergence of the body forces (Kosloff and Baysal, 1982). When the density is constant, equation (1) simplifies to the classical wave equation,

$$\frac{1}{C^2}\frac{\partial^2 P}{\partial t^2} = \frac{\partial^2 P}{\partial x^2} + \frac{\partial^2 P}{\partial y^2} + \frac{\partial^2 P}{\partial z^2} + S. \quad (2)$$

A third version of the acoustic wave equation, the so-called nonreflecting wave equation which highly reduces layer reflections, is obtained from equation (1) after impedance matching (Baysal et al., 1984),

$$\frac{\partial^2 P}{\partial t^2} = C\frac{\partial}{\partial x}\left(C\frac{\partial P}{\partial x}\right) + C\frac{\partial}{\partial y}\left(C\frac{\partial P}{\partial y}\right) + C\frac{\partial}{\partial z}\left(C\frac{\partial P}{\partial z}\right) + C^2 S. \quad (3)$$

Depending upon the application, forward modeling consists of a direct numerical solution of one of the above equations.

Numerical solution method

Computation of each time step commences with the calculation of the right-hand side of equation (1), (2), or (3). For equation (1), spatial partial derivative terms are calculated by (1) forward FFT, (2) multiplication by ik_x, ik_y, or ik_z, (3) inverse FFT, (4) multiplication by $1/\rho$, (5) forward FFT, (6) multiplication by ik_x, ik_y, or ik_z, and (7) inverse FFT. For equation (3), multiplication by C but not by $1/\rho$ is performed. For equation (2), multiplication by $-k_x^2$, $-k_y^2$, or $-k_z^2$ is performed between forward and inverse FFTs. Time integration is performed in two steps. Let $R(x, y, z, n\Delta t)$ represent the value of the appropriate right-hand side for $t = n\Delta t$. The first partial time derivative of the pressure at $t = (n + \frac{1}{2})\Delta t$ is approximated by the following:

$$\frac{\partial P[x, y, z, (n+\frac{1}{2})\Delta t]}{\partial t} = \frac{\partial P[x, y, z, (n-\frac{1}{2})\Delta t]}{\partial t} + \Delta t\, D(x, y, z) R(x, y, z, n\Delta t), \quad (4)$$

where $D(x, y, z)$ is equal to $\rho C^2(x, y, z)$, $C^2(x, y, z)$, or unity for equation (1), (2), or (3), respectively. The pressure at $t = (n + 1)\Delta t$ is then approximated by the following:

$$P[x, y, z, (n+1)\Delta t] = P(x, y, z, n\Delta t) + \Delta t \frac{\partial P[x, y, z, (n+\frac{1}{2})\Delta t]}{\partial t}. \quad (5)$$

Following time stepping, an absorbing boundary is applied to P and $\partial P/\partial t$ on the bottom and lateral edges of the spatial grid. The absorbing boundary is applied as a 15-point weighting function (Cerjan et al., 1985).

For the top boundary, there is an option of introducing a free surface or of allowing events to wrap around to the bottom of the grid and be eliminated by the absorbing boundary. The free-surface condition is approximated by including a wide zone with zero velocity above the upper surface of the model or, equivalently because of periodicity, below the bottom of the model. Since the boundary condition is not specified explicitly, comparison with analytic solutions is required. Computationally, a more accurate solution is achieved by padding zeros at the end of each constant-x or constant-y P vector prior to current time-step computations. Although the FFT length is typically doubled, SSD memory requirements do not change, since temporary central memory storage is used for the zero padded region with each FFT computation step. As in the 2-D case, we could not find any change in the stability requirements when free-surface boundary conditions were introduced. A detailed description of the Fourier method can be found in Gazdag (1981) and in Kosloff and Baysal (1982).

Computer implementation

Let NX, NY, and NZ denote the number of grid points in the x, y, and z directions, respectively. The numerical solution of equation (1) requires four global arrays of size $NX \times NY \times NZ$ for variables P, $\partial P/\partial t$, ρ, and C and, in addition, needs one auxiliary array of the same size for the accumulation of the right-hand side R. The solution of equation (2) or (3) does not require an array for the density ρ. For meaningfully sized seismic modeling problems, the data storage needed can be large. For example, $256 \times 256 \times 256$ spatial grid points require approximately 84 million words of storage for solving equation (1).

The data storage management scheme is based on a pencil structure as shown by Figure 1. Within a given pencil, the above five variables are stored in consecutive memory locations; storage progresses most rapidly in the z direction, then the x direction, and finally the y direction. Within the

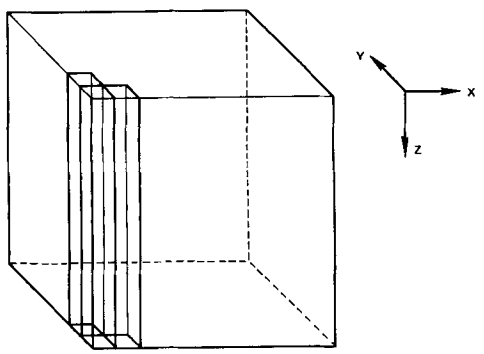

FIG. 1. Pencil data structure. Within the SSD, the left forefront pencil is stored first. Storage progresses in the x-direction and then to pencils in the y-direction. The number of x and y coordinates in each pencil is a program variable. Within each pencil, five variables are grouped in consecutive words; z is the fastest increasing coordinate, followed by x, and then y.

SSD, the storage progresses to the neighboring pencil in the x direction and then to the next row of pencils in the y direction. With the pencil storage, a set of data planes perpendicular to the x-axis (yz planes) or planes perpendicular to the y-axis (xz planes) can be transferred between the SSD and central memory with a small number of input-output operations. Queued input-output operations are used, and a single input-output operating system request is used to transfer a set of yz or xz planes. The size of each pencil is a program variable and a function of available central memory. Pencils containing $8 \times 8 \times 256 \times 5$ words were employed for $256 \times 256 \times 256$ spatial grid point models.

Computation of the first time step, $t = \Delta t$, requires two data passes. At times $t = 0$ and $t = -\frac{1}{2}\Delta t$, P and $\partial P/\partial t$ are initialized to zero. The partial derivative terms with respect to x and z of equation (1), (2), or (3) are computed on all NY xz data planes. The second data pass computes the partial derivative term with respect to y and performs time stepping according to equations (4) and (5) on all NX yz data planes. The absorbing boundary is then applied to P and $\partial P/\partial t$. This completes the computation of the first time step. Prior to passing the yz data planes to the SSD, we progress to the second time step, $t = 2\Delta t$, by computing the partial derivative terms with respect to y and z. The third data pass computes the partial derivative term with respect to x and performs time stepping according to equations (4) and (5) on all NY xz data planes. The second time step is completed after applying the absorbing boundary. We then proceed to the third time step by repeating the calculations of the first data pass prior to passing the xz data planes to the SSD. The numerical scheme continues in the above fashion alternately operating on yz and xz data planes. $N + 1$ retrieval and storage passes of the data are required for computation of N time steps. The various steps of the algorithm are summarized in the schematic diagram shown in Figure 2.

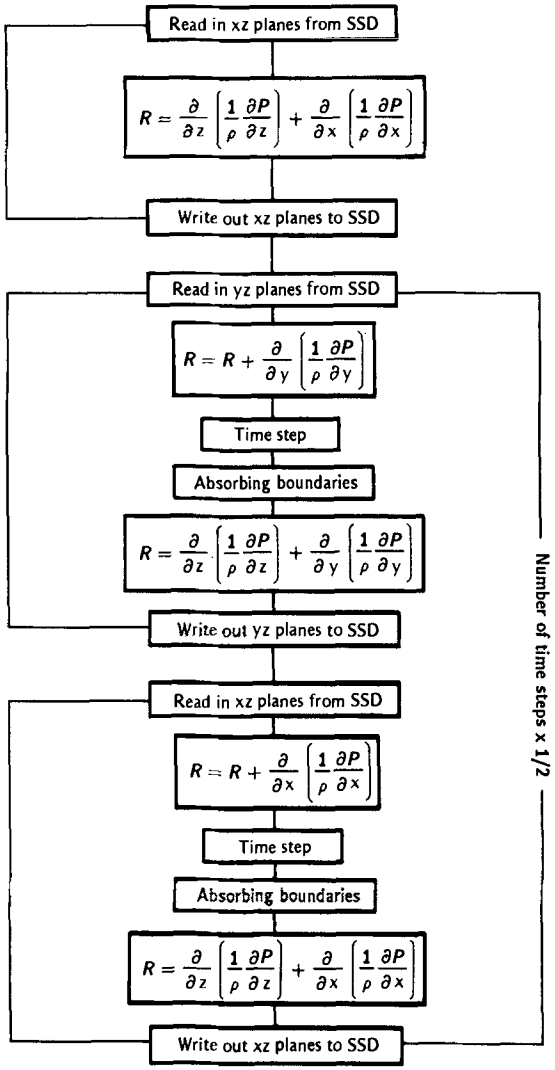

FIG. 2. Schematic diagram of algorithm steps for the variable-density case, assuming an even number of time steps. Not shown is the inclusion of the source term, which is zero except in a region about the source location.

EXAMPLES

Wave propagation for a horizontal interface with a free surface

This and the following example with known analytical solutions test the accuracy of the numerical algorithm. This example features a structure with one horizontal interface and an upper free surface. The modeled region has an approximate size of 5 km $\times$ 5 km $\times$ 2.5 km in the x, y, and z directions, respectively, with a $256 \times 256 \times 128$ spatial grid and grid spacing of 20 m. Velocities are 2000 m/s and 4000 m/s for the upper and lower regions, respectively, with constant density. The source, a band-limited Ricker wavelet (Figure 3a), was applied in the upper layer. The source amplitude spectrum peaks at 25 Hz with significant amplitudes up to 50 Hz (Figure 3b); 50 Hz corresponds to a spatial wavelength of two grid points in the upper region.

Figures 4a–4c represent three snapshots for different times on the zy, zx, and xy planes, respectively. The two vertical zx and zy planes chosen for the display pass through the source. The location of each plane can be seen in the upper right corner of the plots. The events in these figures can be interpreted as the direct wave, the reflected and transmitted waves, the surface multiple, and the reflected multiples. In the zy plane,

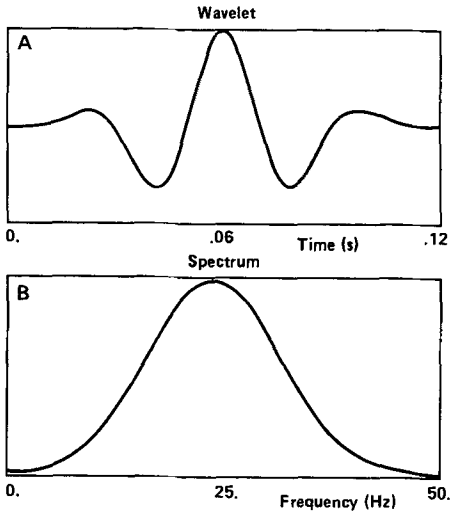

FIG. 3. Source for horizontal interface with a free-surface model.

the direct and reflected waves are represented in the upper region; the transmitted wave travels faster and therefore has a wider wavefront. In the zx plane, note a free-surface reflection. The horizontal snapshot (xy plane) shows perfect circles due to the symmetry of the model. The inner circle is the free-surface reflection, followed by the reflected wave from the material interface. The outer circle represents the direct wave which has almost been absorbed. A different perspective on the wave propagation is contained in the vertical time section of Figure 5.

Figures 6a–6c compare numerical and analytical time histories for the receiver locations given in Figure 7. The analytical solutions are based on the Cagniard-de Hoop method (Aki and Richards, 1980). The figures show that the agreement between numerical and analytical solutions is good. The relatively large disagreement in the third event of Figure 6b is due to the uncertainty of the exact location of an interface within one grid point in the Fourier method and to the simultaneous arrivals of the interface and surface reflections. This example shows that the Fourier method performs well for structures with high velocity contrasts and a free surface. The frequency bandwidth of the source contains appreciable energy with wavelengths as short as two grid points. This is an indication of the accuracy of the Fourier method, at least for structures with horizontal interfaces.

Wave propagation for a dipping interface

This example considers wave propagation in a structure containing a single dipping interface without a free surface. From a mathematical viewpoint, this example is identical to the horizontal interface problem, differing only by a rotation. From a numerical viewpoint, the inclined structure is approximated on the numerical mesh by stair-stepping which can cause spurious diffractions. Some sacrifice in the source frequency content is necessary to reduce the diffractions. The model parameters for this example are identical to those of the preceding example, with the exception of our using a source high-cut frequency of 35 Hz instead of 50 Hz. The dip of the structure is approximately 15 degrees. Figures 8a–8c represent vertical and horizontal snapshots at different times. The location of each snapshot plane is shown in the upper right

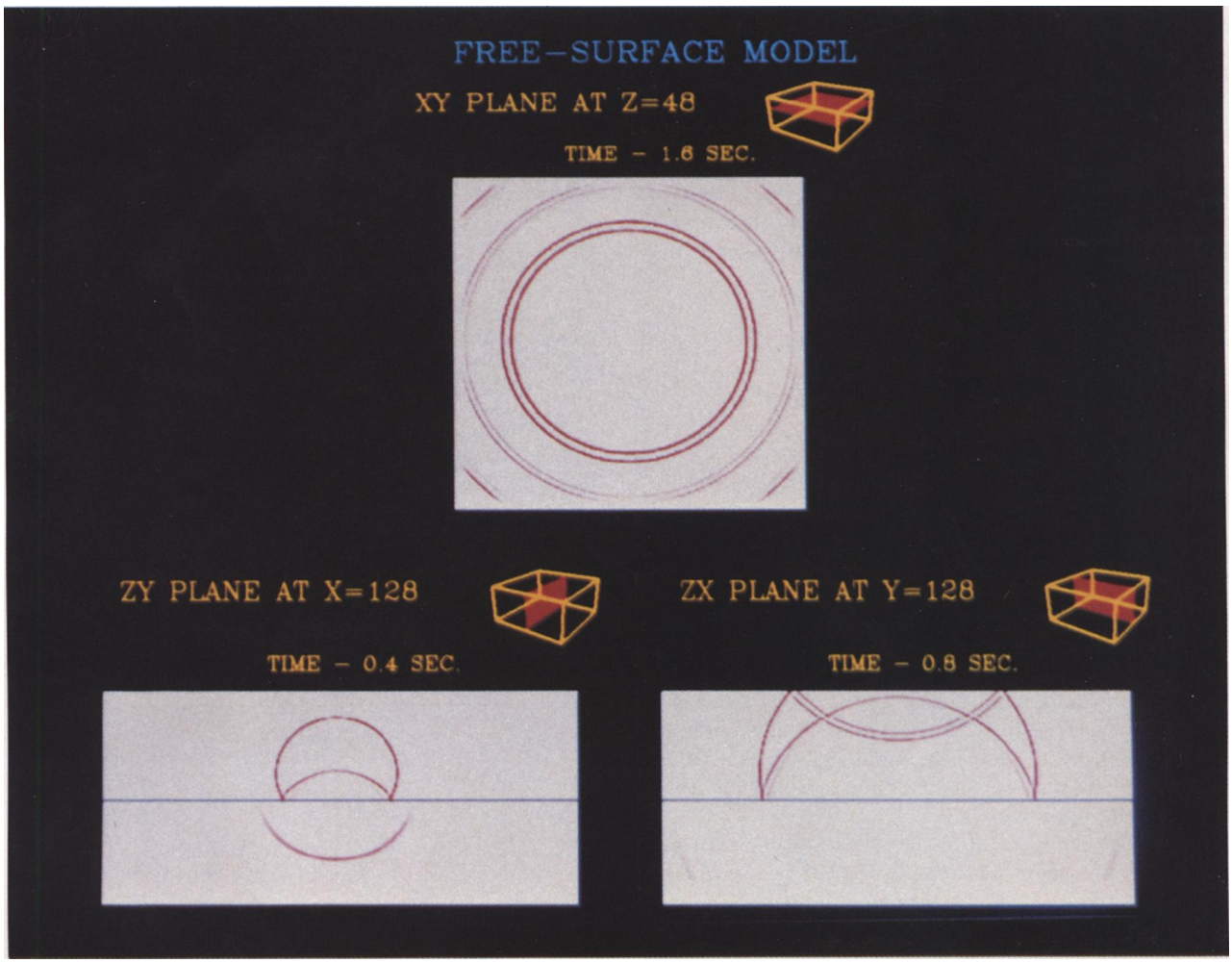

FIG. 4. P-wave snapshots for the free-surface model. The position of each plane within the 3-D volume is shown at the upper right corner. (a)–(c) correspond to lower left, lower right, and upper snapshots, respectively.

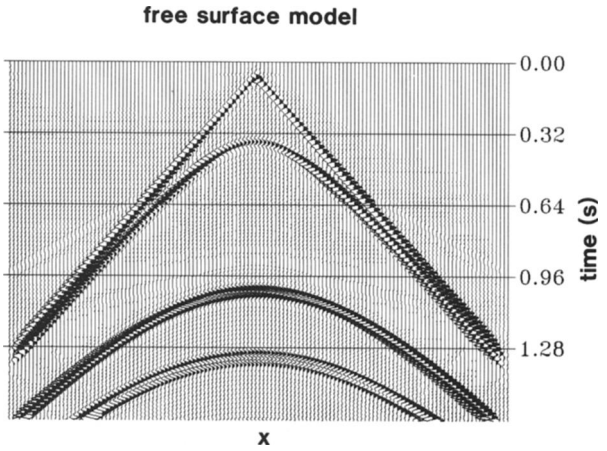

FIG. 5. Free-surface model—time section along the x-axis. With increasing arrival times, events are the direct wave, the reflection from the horizontal interface, the surface multiple, and the reflected multiple. Automatic gain control has been applied.

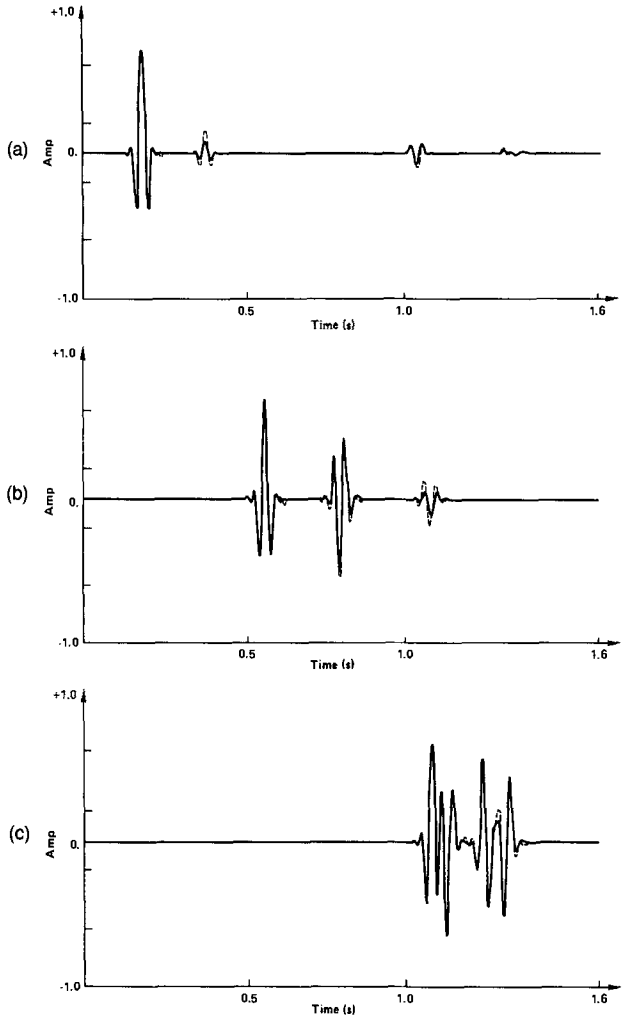

FIG. 6. Free-surface model—numerical and analytical time histories. Numerical and analytical solutions are dashed and solid lines, respectively.

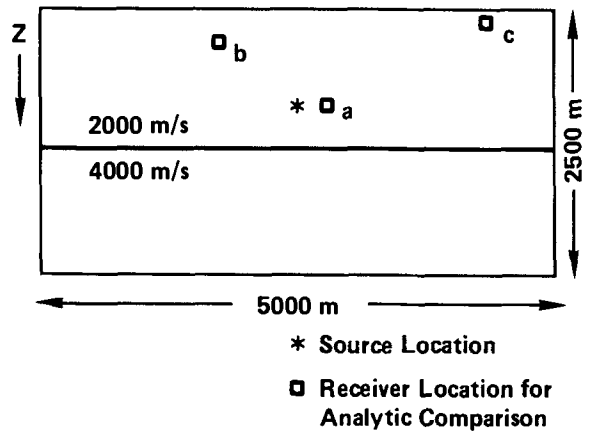

FIG. 7. Free-surface model—location of receivers for numerical and analytical comparisons of Figure 6.

corner. The three events appearing in these figures are the direct, reflected, and transmitted waves. With dip, the reflection is not symmetrical on the horizontal section (Figure 8c). The widening of the wavefront in the high-velocity region can be clearly noted in the zy snapshot. Strike and dip time sections (Figures 9a and 9b) show the direct and reflected arrivals. Figures 10a–10c compare numerical and Cagniard-de Hoop analytical solutions at three receiver locations shown in Figure 11. The agreement is still good, although some diffraction arrivals can be noticed after the reflection arrival. The appearance of the diffractions can be seen very clearly in Figure 9b. A further reduction in the source frequency content would diminish the diffractions at the expense of resolution. The diffractions can also be diminished by decreasing the grid spacing. Doubling the grid resolution increases the number of computations by an order of magnitude. It can be argued that the diffraction issue is a tradeoff between the desired accuracy and computational cost. However, the size of fast accessible computer memory is currently the dominant factor constraining 3-D forward modeling.

Syncline model

This example demonstrates the ability of the modeling algorithm to simulate a zero-offset survey using the exploding reflector method (Loewenthal et al., 1976). The structure consists of a truncated dipping interface which overlies a sharp syncline. This structure was modeled by a 256 × 256 × 128 grid with a grid spacing of 20 m in all three directions. The model configuration and physical parameters are shown in Figure 12. The density is constant, and computations use equation (3). To initiate the forward modeling, the reflectors are exploded at time $t = 0$. The wave field is propagated using half of the acoustic velocity.

Figures 13a and 13b represent snapshots at time $t = 0$ on two perpendicular planes. Figure 13c shows the pressure field on an xz plane at a later time, where the distortion of the reflector's shape can be noticed. The direct arrival from the inclined surface can hardly be noticed, but the two crossing events from the syncline edges are clearly represented. In this type of modeling, amplitudes are not correctly represented. Since the syncline structure does not change along the y-axis,

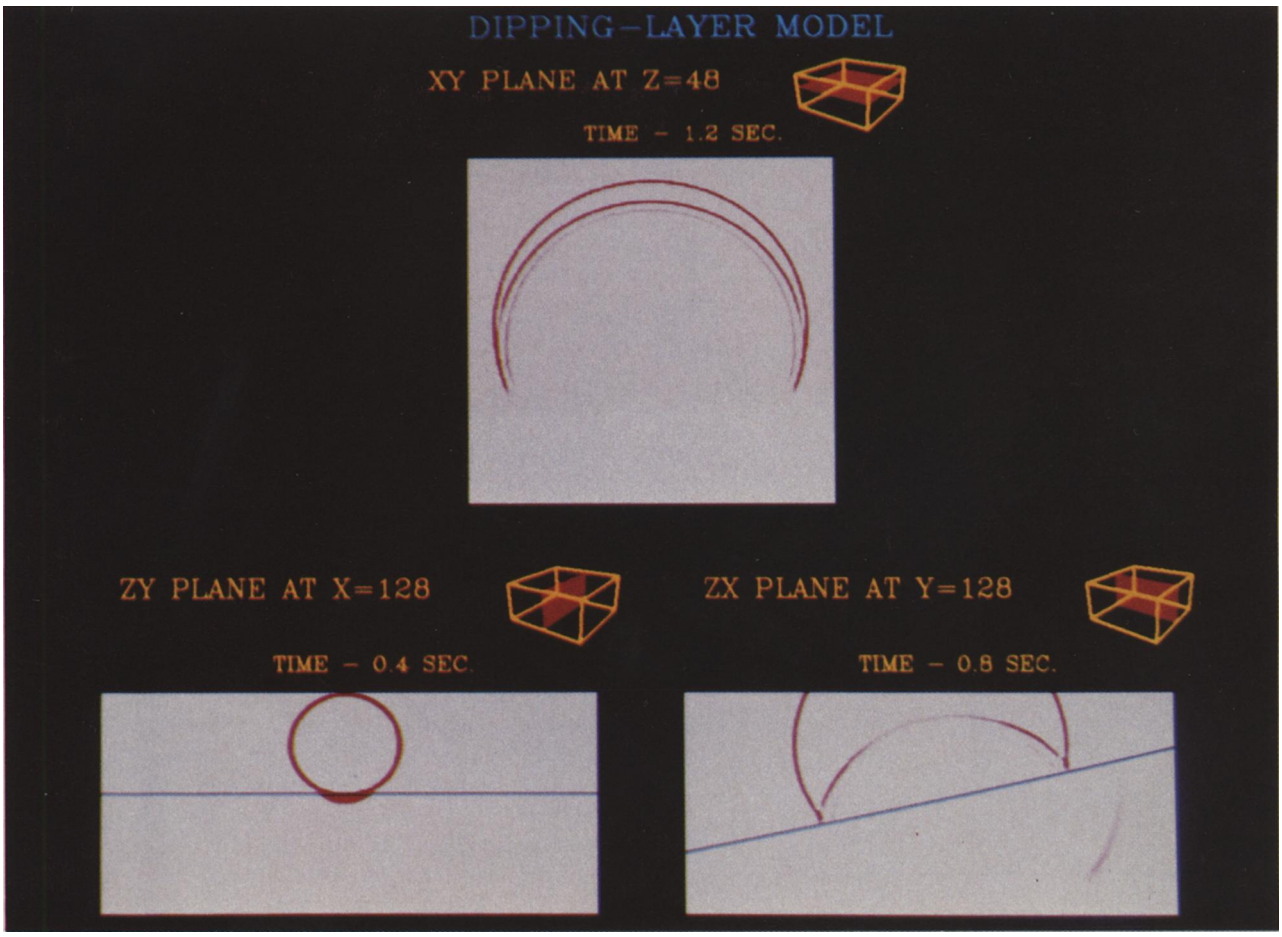

FIG. 8. *P*-wave snapshots for dipping interface model. The position of each plane within the 3-D volume is shown at the upper right corner. (a)–(c) correspond to lower left, lower right, and upper shapshots, respectively.

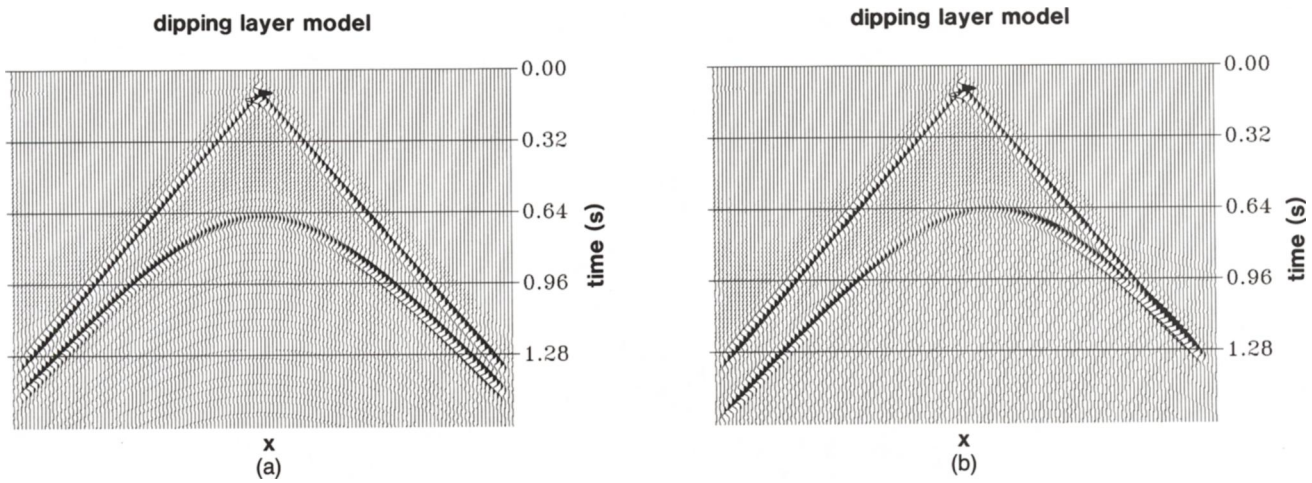

FIG. 9. Dipping interface model—time section along (a) the strike line and (b) the dip line. Events are direct and reflected arrivals. Automatic gain control has been applied.

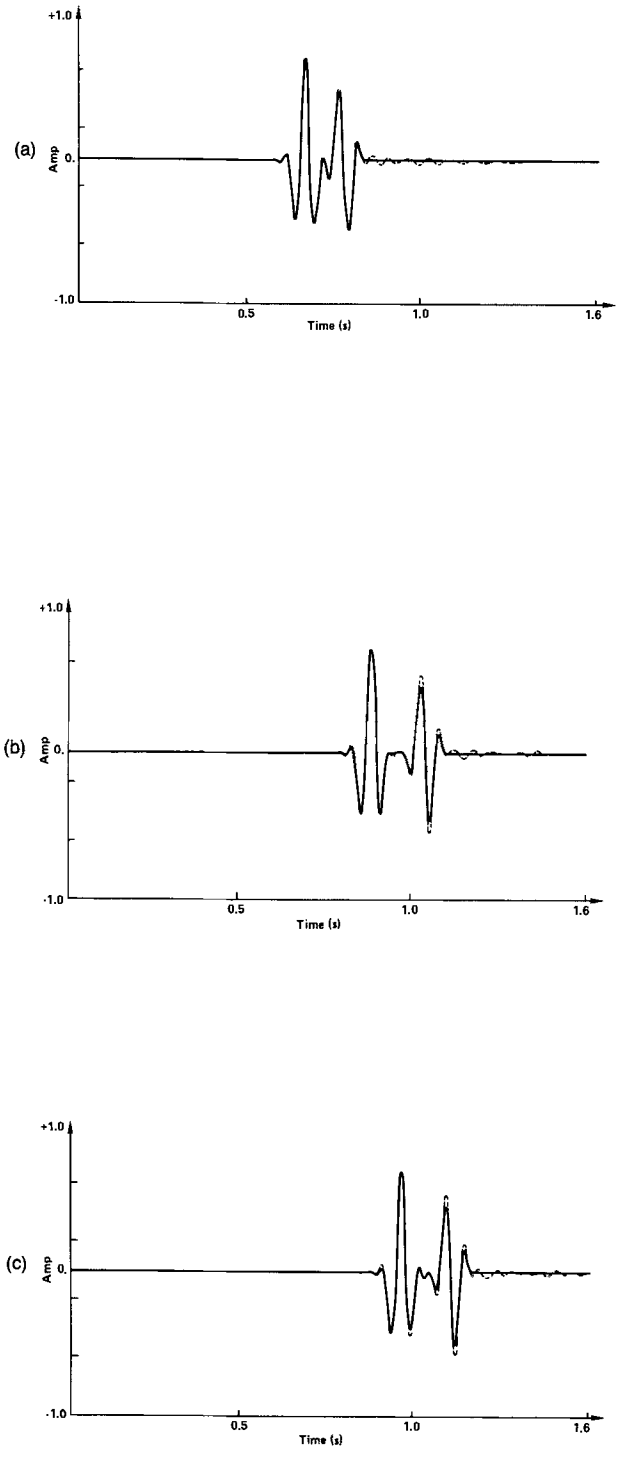

FIG. 10. Dipping interface model—numerical and analytical time histories. Numerical and analytical solutions are dashed and solid lines, respectively.

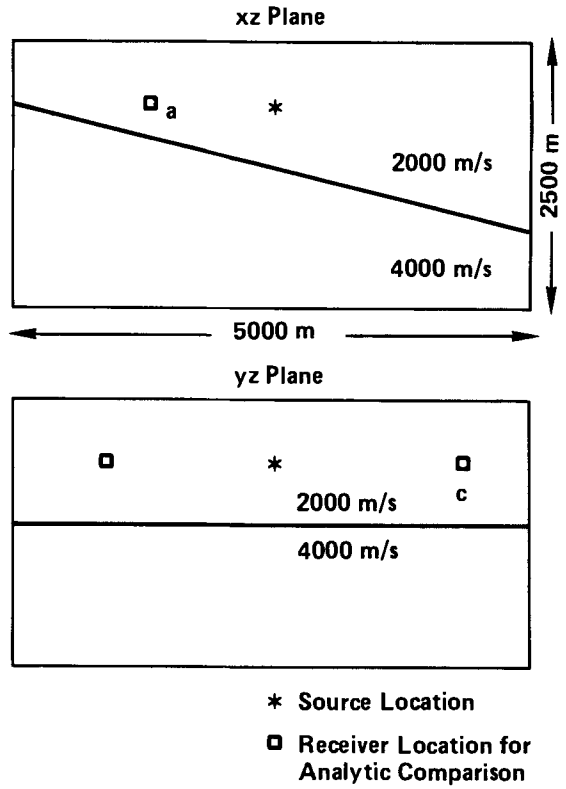

FIG. 11. Dipping interface model—locations of receivers for numerical and analytical comparisons of Figure 10.

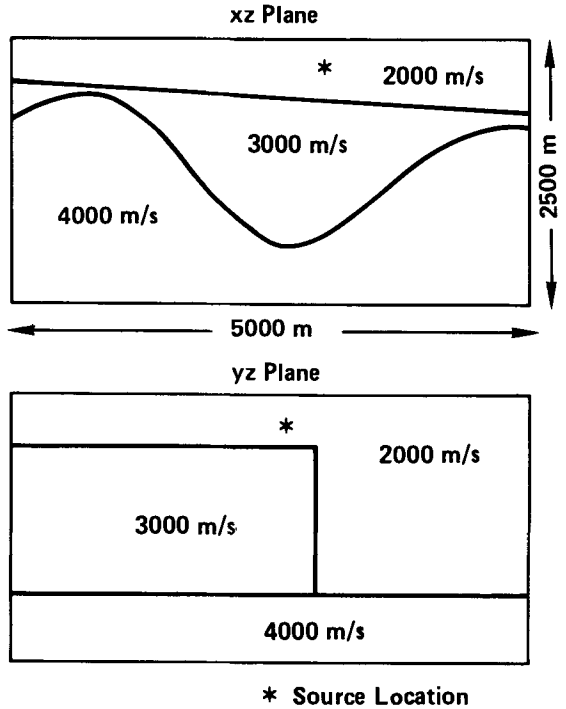

FIG. 12. Syncline model—configuration and physical parameters.

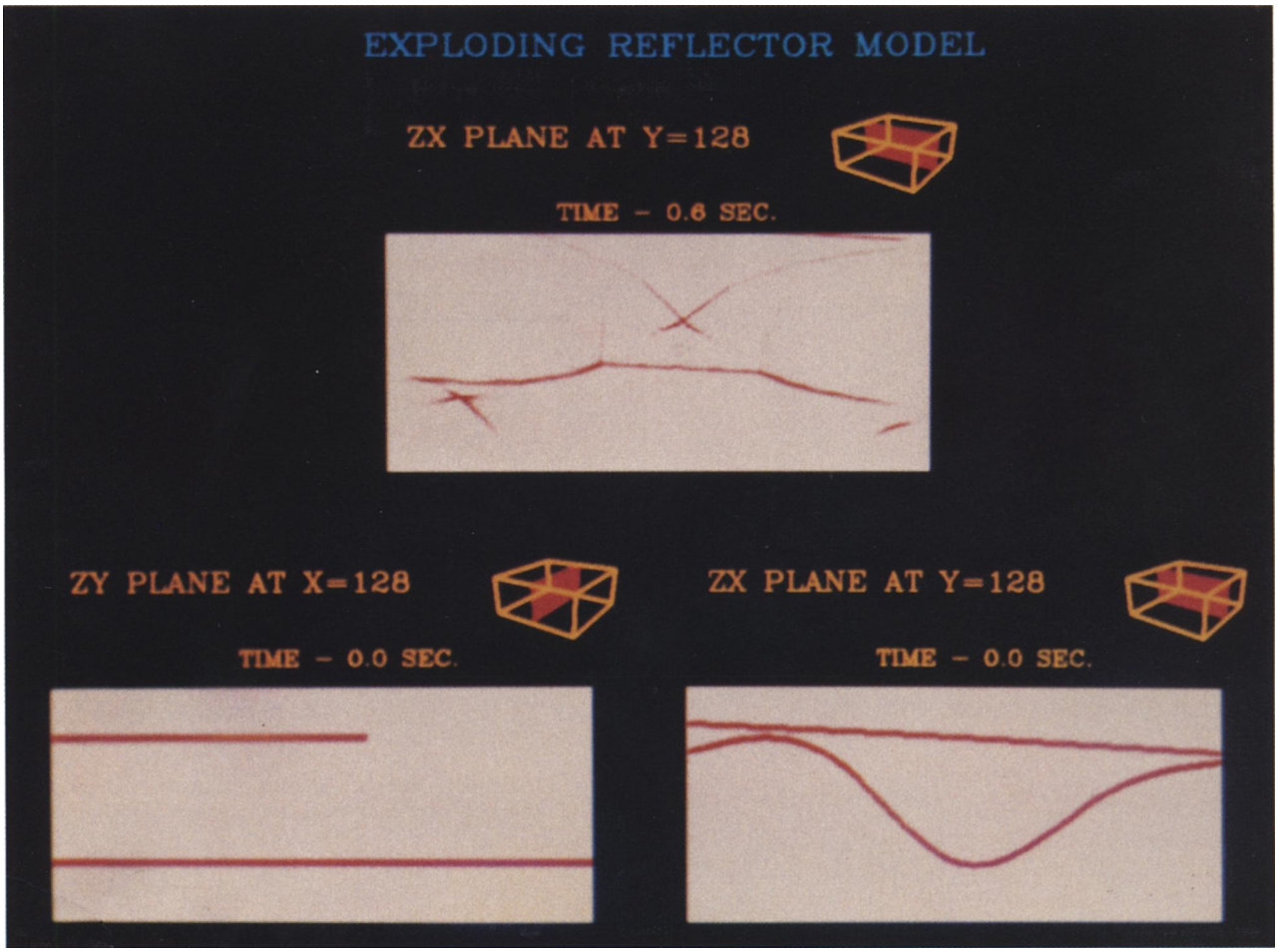

FIG. 13. Syncline model—*P*-wave snapshots for syncline model. The position of each plane with the 3-D volume is shown at the upper right corner. (a)–(c) correspond to lower left, lower right, and upper snapshots, respectively.

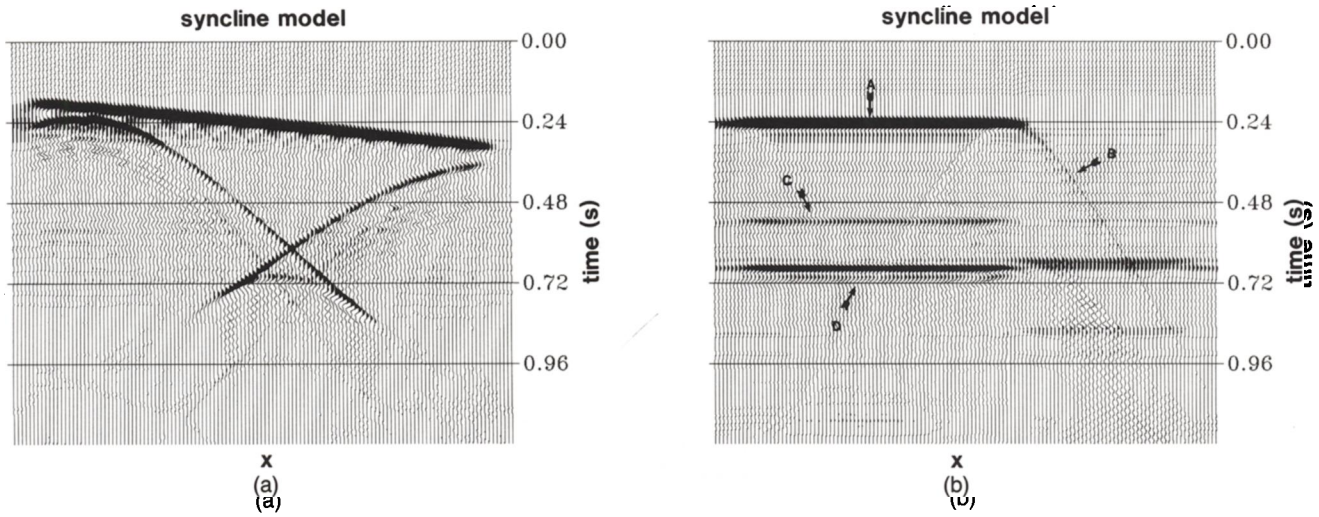

FIG. 14. Syncline model—time section along (a) the *x*-axis and (b) the *y*-axis. Automatic gain control has been applied.

zx time sections, calculated far enough from the truncated interface, will show events which can be modeled with 2-D algorithms. The time section in Figure 14a is such an example. The time section in Figure 14b was calculated along the y-axis immediately above the syncline's deepest extremity and contains out-of-plane events. In this figure, the reflection from the upper interface and the diffraction from the truncation edge are annotated as A and B, respectively. C is an out-of-plane event corresponding to reflection from the syncline wall. Event D is the reflection from the syncline bottom and is broken due to the truncation edge.

CONCLUSIONS

We have presented a 3-D forward modeling algorithm based on a direct solution of the acoustic wave equation. The feasibility of this algorithm has been demonstrated with an implementation on a CRAY X-MP/48 system and an SSD. For example, a model of $256 \times 256 \times 256$ grid points and 1500 time steps (constant-density case) can be calculated within 2 hours of elapsed or wall-clock time using four CPUs. We believe that this algorithm may prove useful for seismic interpretation, especially for structures for which ray-tracing methods fail to give satisfactory results. Comparisons between numerical and analytical solutions lead to the expectation that the modeling algorithm will produce accurate results for more complicated and realistic problems.

Based on the results of this study and the current state of computer technology, we believe that the Fourier method is most effective for 3-D modeling, since it requires fewer grid points to obtain a specified accuracy. This point is especially significant, since, for example, an increase of grid resolution by a factor of two increases both data storage requirements and the number of computations by an order of magnitude. Of greater consequence is the possibility of not having enough fast, accessible memory to model the original problem. The availability of "unlimited" central memory or fast, accessible secondary memory would necessitate our revisiting algorithm implementation and perceived advantages and disadvantages of all forward modeling techniques.

Acoustic forward modeling is a first step in the realistic simulation of wave propagation in the earth. A more realistic simulation can be achieved with 3-D elastic forward modeling (Reshef et al., 1988, this issue).

REFERENCES

Aki, K., and Richards, P. G., 1980, Quantitative seismology, theory and methods, **1**: W. H. Freeman and Co., chap. 6.

Baysal, E., Kosloff, D., and Sherwood, J. W. C., 1984, A two way nonreflecting wave equation: Geophysics, **49**, 132–141.

Cerjan, C., Kosloff, D., Kosloff, R., and Reshef, M., 1985, A nonreflecting boundary condition for discrete acoustic and elastic wave equations: Geophysics, **50**, 705–708.

Gazdag, J., 1981, Modeling of acoustic wave equation by transform methods: Geophysics, **46**, 854–859.

Hilterman, F. J., 1970, Three-dimensional seismic modeling: Geophysics, **35**, 1020–1037.

Kelly, K. R., Ward, R. W., Treitel, S., and Alford, R. M., 1976, Synthetic seismograms: A finite-difference approach: Geophysics, **41**, 2–27.

Kosloff, D., and Baysal, E., 1982, Forward modeling by a Fourier method: Geophysics, **47**, 1402–1412.

Loewenthal, D., Lu, L., Roberson, R., and Sherwood, J. W. C., 1976, The wave equation applied to migration: Geophys. Prosp., **24**, 380–399.

Marfurt, K. J., 1984, Accuracy of finite-difference and finite-element modeling of the scalar and elastic wave equations: Geophysics, **49**, 533–549.

Reshef, M., Kosloff, D., Edwards, M., and Hsiung, C., 1988, Three-dimensional elastic modeling by the Fourier method: Geophysics, **53**, this issue, 1184–1193.